

Study of muon tomographic imaging for high Z material detection with a Micromegas-based tracking system

Liu Cheng-Ming,¹ Wen Qun-Gang,^{2,*} Zhang Zhi-Yong,^{1,†} and Huang Guang-Shun^{1,‡}

Affiliations:

¹State Key Laboratory of Particle Detection and Electronics, University of Science and Technology of China, Hefei 230026, China

²AnHui University, Hefei 230061, China

Abstract: A high spatial resolution tracking system was setup with the Micro-mesh gaseous structure (Micromegas) detectors in order to study the muon tomographic imaging technique for nuclear threat detection. 6 layers of 90 mm × 90 mm one-dimensional readout Micromegas were used to construct a tracking system. The imaging test using some metallic bars was performed with cosmic ray muons. A two-dimensional imaging of the test object was presented with a newly proposed ratio algorithm.

Key words: Muon tomography imaging, Micromegas detector, ratio algorithm, high spatial resolution

1. Introduction

Muon tomography imaging is a new technique developed to reconstruct three-dimensional images of volumes using information from the Coulomb scattering of muons. A well-defined characteristic of this technique using cosmic ray muons is its non-invasiveness and economical value [1, 2]. Since its introduction in the 1950s, Muon tomography imaging has been under development for many purposes, such as detecting nuclear material in road transport vehicles, monitoring cargo containers at custom entrances and potential underground sites used for carbon sequestration.

Muons on Earth are the secondary particles that come from the extensive atmosphere shower of high-energy cosmic rays from space, with a flux about $1 \text{ cm}^{-2}\text{min}^{-1}$ at sea level and an average energy of about 3 GeV. Thus, high efficiency and good spatial resolution tracing detector is required for timely imaging events. For instance, a GEANT4-based simulation shows that better than 200 μm spatial resolution is required for the imaging of a $\phi 200 \text{ mm}$ uranium ball inside a 5 m high cargo container within 10 minutes [3].

A micro-mesh gaseous structure (Micromegas) is a typical Micro-pattern gas detector

(MPGD), which has good spatial resolution of $< 100 \mu\text{m}$, is easy to extend to large area [4, 5]. In this paper, a high spatial resolution tracking system consisting of 6 layer of one-dimensional readout Micromegas detectors is setup to study the muon imaging method for high-Z materials. The schematic design, detector and electronics, data acquisition (DAQ) of the test system is demonstrated. A new ratio algorithm is introduced and applied on the real data. A two-dimensional imaging of a test object is finally obtained.

2. Tracking system

2.1. Schematic design

In this tracking system, two $150 \text{ mm} \times 150 \text{ mm}$ scintillators are used to select effective events that penetrate the whole tracking detectors and provide trigger signals for the DAQ by coinciding their signals. Six layers of $90 \text{ mm} \times 90 \text{ mm}$ one-dimensional readout Micromegas detectors are used to determine the tracks of incident and exiting muons from a test object. As shown in Figure 1, the detectors 4-6 are for the tracking of incident muons; detectors 1-3 are for exiting muons scattered by the nuclei of the test object. Signals of the Micromegas detectors are readout by front-end electronics with APV25 ASICs [6] and digitized by MPD data acquisition system [7].

The test object consists of four layers of different metallic bars including copper, iron, aluminum and lead, with the Z values of 64, 56, 27 and 207, respectively. Each layer has the same three metallic bars with a size of $10 \text{ mm} \times 10 \text{ mm} \times 100 \text{ mm}$. In other words, it is a 30 mm width, 40 mm high, and 100 mm long test object in total, and is placed along the readout strips of Micromegas detectors.

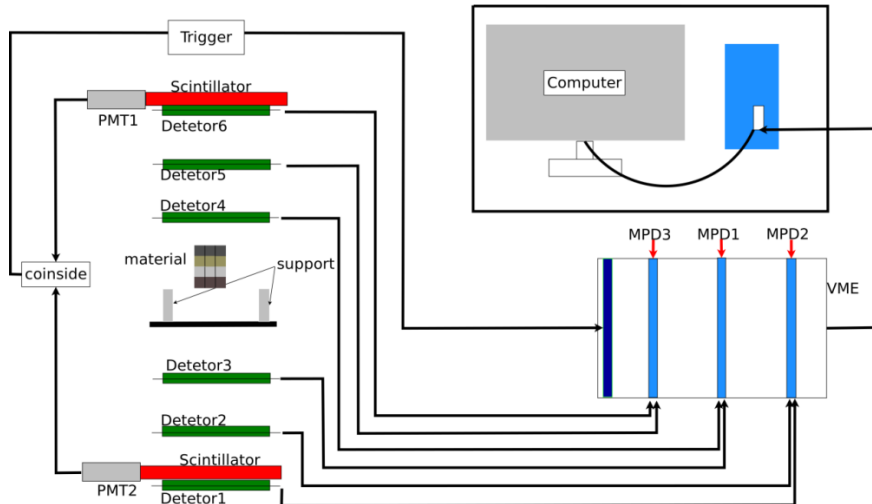


Figure 1. Schematic design diagram for muon imaging study

2.2. Setup of the system

The Micromegas detectors are manufactured using the thermal bonding method [8, 9]. A resistive anode is employed to enhance the gas gain to higher than 10^4 . The readout of detectors is designed as one-dimensional strips with a pitch of $412\text{ }\mu\text{m}$ and drift region of 5 mm , As a consequence, better than $150\text{ }\mu\text{m}$ spatial resolution and higher than 90% detection efficiency are obtained for the cosmic ray muons. As shown in Figure 2, each Micromegas detector is installed in an aluminum plane, where a $100\text{ mm} \times 100\text{ mm}$ hollow hole under the active area of detector is made to minimize the scattering materials in the tracker of muons.



Figure 2. Installation of the tracking system for a single detector

The six detector planes are subsequently stacked to construct the tracking system as the schematic design mentioned above. Figure 3 is the finished view of the installation of Micromegas detectors, and the test object is inserted in the middle of the tracking system. Finally, the whole system is calibrated and aligned with cosmic test, and effective muon events are collected for imaging analysis.

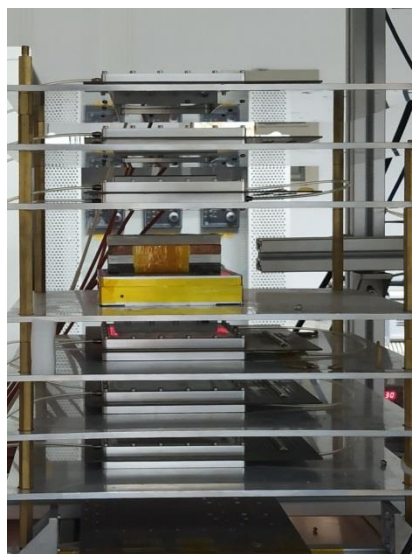


Figure 3. The finished view of installation of the tracker detectors

3. Imaging with the cosmic ray muons

3.1. Ratio algorithm for imaging

In this experiment, a new Ratio Algorithm is proposed for imaging with the effective muon events, based on the idea of finding the cross point of incident and ejected tracks. The deflection angle θ of muons passing through the material approximates a Gaussian distribution with a mean value of zero, as Equation 1 shows. Equation 2 gives an expression to a root mean square error σ_θ , where L is the length of a muon's track in a certain material, L_{rad} the radiation length of the material. The commonly used empirical formula is defined as Equation 3, where Z and A are the atomic number and atomic weight of the substance, respectively, while β , c , p are the Lorentz parameters, the velocity of light, and the momentum of muons, respectively.

$$f(\theta) = \frac{1}{\sqrt{2\pi}\sigma_\theta} \exp\left(-\frac{\theta^2}{2\sigma_\theta^2}\right) \quad (1)$$

$$\sigma_\theta = \frac{13.6 \text{ MeV}}{\beta c p} \sqrt{\frac{L}{L_{rad}}} \left[1 + 0.038\left(\frac{L}{L_{rad}}\right)\right] \quad (2)$$

$$L_{rad} = \frac{716.4 \cdot A}{Z(Z+1)\ln(287/\sqrt{Z})} [\text{g/cm}^3] \quad (3)$$

For a certain L value, as the Z value of the atomic sub-order increases, the radiation length L_{rad} of the material decreases. The σ_θ increases accordingly. The H value, therefore, yields Equation 4:

$$H = \frac{13.6 \text{ MeV}}{\beta c} \sqrt{\frac{L}{L_{rad}}} \left[1 + 0.038\left(\frac{L}{L_{rad}}\right)\right], \quad (4)$$

Equation 2 can subsequently be written like Equation 5:

$$\sigma_\theta^2 = \frac{1}{p^2} H^2 \quad (5)$$

For a distribution with a mean value of zero, its root mean square error can be obtained by fitting the experiment data into Equation 6, where the θ_i represents the measured scattering angle of the number i of muon events in the data, and N the total number of events.

$$\sigma_{\theta}^2 = \frac{1}{N} \sum_{i=1}^N \theta_i^2 \quad (6)$$

Next, we test an object which has a certain H value and whose N events can be divided into n groups according to the momenta of muons. For a group of muons in momentum bin p_i ($i=1, 2 \dots n$), we suppose there are k_i events with scattering angle $\theta_1, \theta_2 \dots \theta_{k_i}$. A series of the root mean square errors can be obtained through Equation 5 and 6:

$$\begin{aligned} \sigma_1^2 &= \frac{1}{k_1} \sum_{i=1}^{k_1} \theta_i^2 = \frac{1}{p_1^2} H^2 \\ \sigma_2^2 &= \frac{1}{k_2} \sum_{i=1}^{k_2} \theta_i^2 = \frac{1}{p_2^2} H^2 \\ &\dots \\ \sigma_n^2 &= \frac{1}{k_n} \sum_{i=1}^{k_n} \theta_i^2 = \frac{1}{p_n^2} H^2 \end{aligned}$$

Rearranging these equations leads to Equation 7, where the coefficient $\frac{k_i}{N}$ indicates the probability of muons in momentum bin p_i .

$$\sigma_{\theta}^2 = \frac{1}{N} \sum_{i=1}^N \theta_i^2 = \sum_{i=1}^n \frac{k_i}{N} \frac{1}{p_i^2} H^2 \quad (7)$$

The flux of muons at different zenith angles decreases sharply with the momenta of muons going up^[10], such that the term $\sum_{i=1}^n \frac{k_i}{N} \frac{1}{p_i^2}$ can be considered as a constant value A when N is large enough. Equation 7 consequently becomes:

$$\sigma_{\theta}^2 = \frac{1}{N} \sum_{i=1}^N \theta_i^2 = \sum_{i=1}^n A H^2 \quad (8)$$

Compared to Equation 5, the influence to root mean square error from the momenta of muons is negligible.

A typical algorithm that gets the root mean square error of scattering angles based on Equation 6 is the point of closest approach (PoCA)^[11]. Due to the term, which sums the square of the scattering angle, PoCA is sensitive to large angle events. In order to eliminate the effect of large angle and obtain good quality of imaging, it is necessary to constrain the angle range.

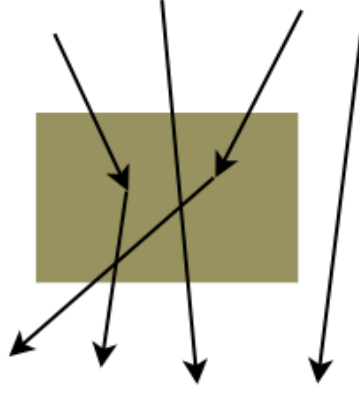


Figure 4. Muon event pass through the test object

To avoid the influence of large angle events, the so-called Ratio Algorithm was proposed. Figure 4 shows the behavior of muons passing through the test object. As mentioned in this paper, the deflection angle obeys Gaussian distribution as Figure 5 shows, the red line indicating the angle distribution of muons passing through the low atomic number Z material, while the blue line relates to the high Z material. As all the events detected are counted as A_0 , and events in certain angle range such as $|\theta| < \theta_0$ are counted as A_c . The ratio R value is defined as Equation 9

$$R = \frac{A_c}{A_0} \quad (9)$$

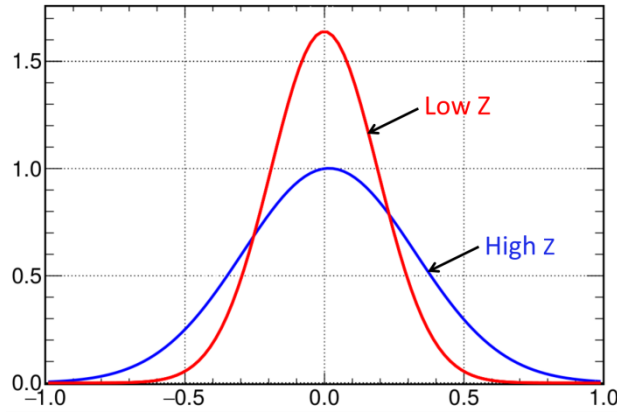


Figure 5. The Gaussian distribution of muon deflection angles in different materials

The ratio value is actually the Gaussian function definite integral (or likelihood error function) of the root mean square error σ_θ , as shown in Equation 10:

$$R(\sigma_\theta) = \frac{1}{\sqrt{2\pi}\sigma_\theta} \int_{-\theta_0}^{\theta_0} \exp\left(-\frac{\theta^2}{2\sigma_\theta^2}\right) d\theta \quad (10)$$

Obviously, for materials with different Z value, the higher Z material has smaller R

value. In this way, different materials can be distinguished. Furthermore, the R value could also be linked to the Z value if the tracking were precise enough.

3.2. Evaluation with real data

The ratio algorithm is proposed for eliminating the effects of large angle events. It is subsequently applied to experimental data. As shown in Figure 6, the schematic diagram of the test system with the test object and the positions along the y-axis are measurable. When muons are scattered by a test object passing by all of the six detectors, the position of the x-axis can be obtained through the detector readout. The incident and ejection tracks can subsequently be reconstructed and, as a result, the two-dimensional position of the exact scatter point is found. For Imaging of the test object, ratios for all points in the measurement area are needed. As an example, the ratio at point A in Figure 6 is calculated through the following steps:

- Take a square exploration area with point A, as its center. Here the exploration area is $33 \text{ mm} \times 33 \text{ mm}$.
- All events passing through the exploration area are counted as A_0 , and events with scatter angles in a certain range ($|\theta| < 1.6^\circ$ in this work) are counted as A_c .
- Use Equation 9 to get the ratio R.

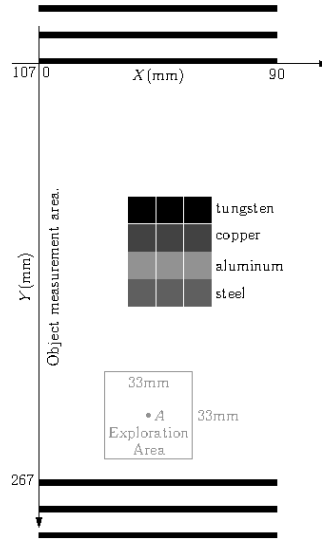


Figure 6. The Diagram of the description of the Ratio Algorithm

In order to ensure the unbiased R values, 500,000 points were selected randomly in the test object measurement area, and the R values were calculated for all points. Consequently, a quantity field $R(x, y)$ (i.e. the R value with coordinates around point A) of the object measurement area is obtained. In this way, the image of cosmic-ray

muon tomography is visualized using ratios, as shown in Figure 7. The rectangular box with coordinates shows the location and size of the test object. These points with ratio less than 0.800 are roughly formed into a rectangle. The reconstructed rectangle is smaller than the

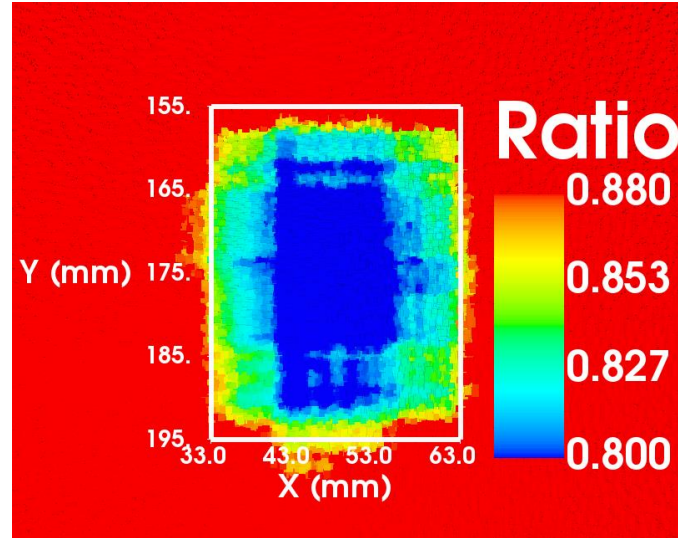


Figure 7. The image of test object by cosmic ray muon tomography actual test object, but the reconstructed position is consistent with the actual position. Besides, these points with a ratio greater than 0.880 represent the air. The ratio value from 0.800 to 0.880 mainly occurs in the transition region between the test object (high-Z) and air (low-Z). In this system, the reconstruction uses data from 793 effective muons detected in one day, with a detection flux about 10 cm⁻² day⁻¹. The lower detection flux is due to removing the noised events. Improving detection flux will be very useful for rapid detection to some extend.

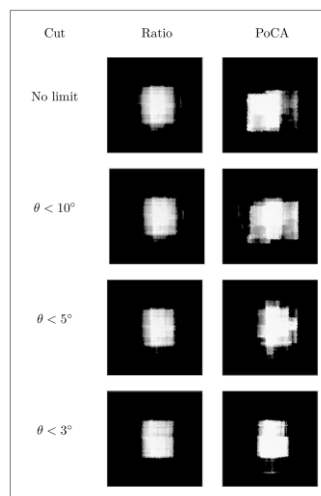


Figure 8. Comparison of Ratio and PoCA after the different angle limits
As mentioned earlier, constraining the scattered angle to suppress the effect of large

angles is one feature of PoCA. These two algorithms are applied under different scatter angle θ cuts, as shown in Figure 8. It can be seen that more stringent angle cuts bring better imaging quality for PoCA, but less influence to Ratio.

Discussion

The tomographic imaging is realized. More work needs to be done to apply the system to high Z material detection. The goal of three-dimensional tomographic imaging is set and the research and development of two-dimensional Micromegas detectors is in progress, as well as the improvement of the algorithm. The ability to distinguish different materials is also promising.

Acknowledgements

This work was supported by the Program of National Natural Science Foundation of China Grant No. 11605197, the Fundamental Research Funds for the Central Universities, and the State Key Laboratory of Particle Detection and Electronics, SKLPDE-ZZ-201818, SKLPDE-KF-201912. This work was partially carried out at the USTC Center for Micro and Nanoscale Research and Fabrication, and we wish to thank Yu Wei for his help on the nanofabrication steps for germanium coating.

References

- 1 Tanaka H K M, Nakano T, Takahashi S, et al. Development of an emulsion imaging system for cosmic-ray muon radiography to explore the internal structure of a volcano, Mt. Asama[J]. Nuclear Instruments and Methods in Physics Research Section A: Accelerators, Spectrometers, Detectors and Associated Equipment, 2007, 575(3): 489-497.
- 2 Jonkmans, G., et al. "Nuclear waste imaging and spent fuel verification by muon tomography." Annals of Nuclear Energy 53 (2013): 267-273.
- 3 Hohlmann M, Ford P, Gnanvo K, et al. GEANT4 Simulation of a Cosmic Ray Muon Tomography System With Micro-Pattern Gas Detectors for the Detection of High-Z Materials[J]. IEEE Transactions on Nuclear Science, 2009, 56(3): 1356-1363.
- 4 Giomataris, Yannis, et al. "MICROMEAS: a high-granularity position-sensitive gaseous detector for high particle-flux environments." Nuclear Instruments and Methods in Physics Research Section A: Accelerators, Spectrometers, Detectors and Associated Equipment 376.1 (1996): 29-35.
- 5 Iodice, Mauro. "Micromegas detectors for the Muon Spectrometer upgrade of the

- ATLAS experiment." Journal of Instrumentation 10.02 (2015): C02026.
- 6 French M J, Jones L L, Morrissey Q, et al. Design and results from the APV25, a deep sub-micron CMOS front-end chip for the CMS tracker[J]. Nuclear Instruments and Methods in Physics Research Section A: Accelerators, Spectrometers, Detectors and Associated Equipment, 2001, 466(2): 359-365.
 - 7 MPD collaboration, "MPD Conceptual Design Report v1.4," tech. rep., JINR, Dubna, 2013.
 - 8 L. Guan et al., Micromegas prototypes with thermo-bond film separators, Chinese Phys. C 35 (2011)163.
 - 9 Z.Y. Zhang, et al., Journal of Instrumentation, Volume 9, October 2014, C10028.
 - 10 Tsuji S, Katayama T, Okei K, et al. Measurements of muons at sea level[J]. Journal of Physics G: Nuclear and Particle Physics, 1998, 24(9): 1805.
 - 11 Schultz L J, Borozdin K N, Gomez J J, et al. Image reconstruction and material Z discrimination via cosmic ray muon radiography[J]. Nuclear Instruments and Methods in Physics Research Section A: Accelerators, Spectrometers, Detectors and Associated Equipment, 2004, 519(3): 687-694.